Inorg. Chem. **2004**, *43*, 5231–5236

A Large Thermal Hysteresis Loop Produced by a Charge-Transfer Phase Transition in a Rubidium Manganese Hexacyanoferrate

Hiroko Tokoro,[†] Shin-ichi Ohkoshi,*[,†,‡] Tomoyuki Matsuda,[†] and Kazuhito Hashimoto*[,†]

Research Center for Advanced Science and Technology, The University of Tokyo, 4-6-1 Komaba, Meguro-ku, Tokyo, 153-8904, Japan, and PRESTO, JST, 4-1-8 Honcho Kawaguchi, Saitama, Japan

Received December 5, 2003

In a rubidium manganese hexacyanoferrate, $RbMn[Fe(CN)_6]$, the magnetic susceptibility (χ_M) decreased at 225 K ($=T_{1/2\downarrow}$) and abruptly increased at 300 K ($=T_{1/2\uparrow}$) in the cooling and warming processes, respectively. X-ray photoelectron spectroscopy and infrared spectroscopy indicated that the high-temperature (HT) and low-temperature (LT) phases were composed of Mn^{II}–NC–Fe^{III} and Mn^{III}–NC–Fe^{II}, respectively. A structural change from cubic ($F\bar{4}3m$, $a = 10.533$ Å) to tetragonal ($I\bar{4}m2$, $a = b = 7.090$ Å, $c = 10.520$ Å) accompanied the phase transition, and, on the basis of these results, the HT and LT phases were assigned to $Mn^{II}(t_{2g}^3e_g^2, {}^6A_{1g}; S = {}^5/_2)$–NC–$Fe^{III}$ (t_{2g}^5, ${}^2T_{2g}$; $S = {}^1/_2$) and $Mn^{III}(e_g^2b_{2g}^1a_{1g}^1, {}^5B_{1g}; S = 2)$–NC–$Fe^{II}$ ($b_{2g}^2e_g^4$, ${}^1A_{1g}$; $S = 0$), respectively. This phenomenon is caused by a metal-to-metal charge transfer from Mn^{II} to Fe^{III} and a Jahn–Teller distortion of the produced Mn^{III} ion. The reaction mechanism is discussed, considering the entropy difference between the HT and LT phases.

1. Introduction

Thermal phase transition phenomena, which are divided into categories such as spin crossover[1,2] and intramolecular electron transfer, are extensively investigated in solid state chemistry.[1−13] Depending on the strength of the ligand field, a transition metal ion in a spin crossover complex can be in either a low-spin or a high-spin state. When the thermal energy is close to the exchange energy, which corresponds

* To whom correspondence should be addressed. E-mail: ohkoshi@light.t.u-tokyo.ac.jp (S.O.); hashimoto@light.t.u-tokyo.ac.jp (K.H.).
† The University of Tokyo.
‡ PRESTO, JST.

(1) (a) Goodwin, H. A. *Coord. Chem. Rev.* **1976**, *18*, 293. (b) Gütlich, P. *Struct. Bonding (Berlin)* **1981**, *44*, 83. (c) Gütlich, P.; Hauser, A. *Coord. Chem. Rev.* **1990**, *97*, 1. (d) Kahn, O. *Molecular Magnetism*; VCH: New York, 1993. (e) Kahn, O.; Kröber, J.; Jay, C. *Adv. Mater.* **1992**, *4*, 718. (f) Kahn, O.; Martinez, J. C. *Science* **1998**, *279*, 44.
(2) (a) Létard, J. F.; Guionneau, P.; Codjovi, E.; Lavastre, O.; Bravic, G.; Chasseau, D.; Kahn, O. *J. Am. Chem. Soc.* **1997**, *119*, 10861. (b) Renovitch, G. A.; Baker, W. A. *J. Am. Chem. Soc.* **1967**, *89*, 6377. (c) Maeda, Y.; Oshio, H.; Takashima, Y.; Mikuriya, M.; Hidaka, M. *Inorg. Chem.* **1986**, *25*, 2958.
(3) (a) Brown, D. B. *Mixed Valence Compounds*; NATO ASI; Reidel: Dordrecht, 1980. (b) Prassides, K. *Mixed Valency Systems: Applications in Chemistry, Physics and Biology*; NATO ASI; Kluwer: Dordrecht, 1991. (c) Robin, M. B.; Day, P. *Adv. Inorg. Chem. Radiochem.* **1967**, *10*, 247. (d) Hush, N. S. *Prog. Inorg. Chem.* **1967**, *8*, 391. (e) Hendrickson, D. N. *Mixed Valency Systems: Applications in Chemistry, Physics and Biology*; Kluwer: Boston, 1991. (f) Piepho, S. B.; Krausz, E. R.; Schatz, P. N. *J. Am. Chem. Soc.* **1978**, *100*, 2996. (g) Borshch, S. A.; Prassides, K. *J. Phys. Chem.* **1996**, *100*, 9348.
(4) (a) Launay, J. P.; Babonneau, F. *Chem. Phys.* **1982**, *67*, 295. (b) Borshch, S. A.; Kotov, I. N.; Bersuker, I. B. *Chem. Phys. Lett.* **1982**, *89*, 381.
(5) (a) Cannon, R. D.; Montri, L.; Brown, D. B.; Marshall, K. M.; Elliot, C. M. *J. Am. Chem. Soc.* **1984**, *106*, 2591. (b) Sorai, M.; Kaji, K.; Hendrickson, D. N.; Oh, S. M. *J. Am. Chem. Soc.* **1986**, *108*, 702. (c) Jang, H. J.; Vincent, J. B.; Nakano, M.; Huffman, C.; Christou, G.; Sorai, M.; Wittebort, R. J.; Hendrickson, D. N. *J. Am. Chem. Soc.* **1989**, *111*, 7778.
(6) (a) Kitagawa, H.; Onodera, N.; Sonoyama, T.; Yamamoto, M.; Fukuwa, T.; Mitani, T.; Seto, M.; Maeda, Y. *J. Am. Chem. Soc.* **1999**, *121*, 10068. (b) Kitagawa, H.; Mitani, T. *Coord. Chem. Rev.* **1999**, *190*, 1169.
(7) (a) Kojima, N.; Aoki, W.; Seto, M.; Kobayashi, Y.; Maeda, Y. *Synth. Met.* **2001**, *121*, 1796. (b) Kojima, N.; Aoki, W.; Itoi, M.; Ono, Y.; Seto, M.; Kobayashi, Y.; Maeda, Y. *Solid State Commun.* **2001**, *120*, 165.
(8) Jung, O. S.; Jo, D. H.; Lee, Y. A.; Conklin, B. J.; Pierpont, C. G. *Inorg. Chem.* **1997**, *36*, 19.
(9) (a) Sato, O.; Einaga, Y.; Iyoda, T.; Fujishima, A.; Hashimoto, K. *J. Phys. Chem. B* **1997**, *101*, 3903. (b) Shimamoto, N.; Ohkoshi, S.; Sato, O.; Hashimoto, K. *Inorg. Chem.* **2002**, *41*, 678.
(10) (a) Puertolas, J. A.; Navarro, R.; Palacio, F.; Gonzalez, D.; Carlin R. L.; van Duyneveldt, A. J. *J. Magn. Magn. Mater.* **1983**, *31*, 1067. (b) Puertolas, J. A.; Orera, V. M.; Palacio, F.; van Duyneveldt, A. J. *Phys. Lett.* **1983**, *98A*, 374.
(11) Zimmermann, R. *J. Phys. Chem. Solids* **1983**, *44*, 151.
(12) (a) Kambara, T. *J. Phys. Soc. Jpn.* **1980**, *49*, 1806. (b) Sasaki, N.; Kambara, T. *J. Chem. Phys.* **1981**, *74*, 3472. (c) Kambara, T. *J. Chem. Phys.* **1981**, *74*, 4557.
(13) (a) Ohnishi, S.; Sugano, S. *J. Phys.* **1981**, *C14*, 39. (b) Spiering, H.; Meissner, E.; Köppen, H.; Müller, E. W.; Gütlich, P. *Chem. Phys.* **1982**, *68*, 65. (c) Boukheddaden, K.; Shteto, I.; Hôo, B.; Varret, F. *Phys. Rev. B* **2000**, *62*, 14796. (d) Boukheddaden, K.; Linares, J.; Codjovi, E.; Varret, F.; Niel, V.; Real, J. A. *J. Appl. Phys.* **2003**, *93*, 7103.

10.1021/ic030332f CCC: $27.50
Published on Web 07/20/2004

to the crossover, a spin transition occurs between the two spin states and is typically observed in octahedral coordinate iron transition metal complexes.[2] Another category is the charge-transfer phase transition, which has been observed in mixed-valence complexes,[3−6] and charge-transfer phase transitions accompanied by spin crossovers have also been reported. For example, in $(n\text{-}C_3H_7)_4N[Fe^{II}Fe^{III}(dto)_3]$ (dto = $C_2O_2S_2$), the $Fe^{III}(S = {}^1/_2)-Fe^{II}(S = 2)$ phase converts to the $Fe^{II}(S = 0)-Fe^{III}(S = {}^5/_2)$ phase.[7] $Co(py_2X)(3,6\text{-}DBQ)_2$ (X = O, S, Se)[8] and $Na_{0.4}Co_{1.3}[Fe(CN)_6]\cdot 4.9H_2O$[9] were also reported to have this type of charge-transfer transition. Often, a thermal phase transition accompanies a thermal hysteresis loop.[7−9] A thermal hysteresis loop is related to the cooperativity of the corresponding system and in a metal complex assembly is due to the interaction between a metal ion and lattice strain. Examples include electron−phonon coupling,[11] Jahn−Teller distortions,[12] and elastic interactions.[13] Since cyano-bridged metal assemblies[14,15] such as Prussian blue analogues are mixed-valence compounds with a strong cooperativity due to the bridged CN^- ligand, they are suitable for observing thermal phase transitions. We have recently observed a temperature-induced phase transition with a large thermal hysteresis loop in rubidium manganese hexacyanoferrate.[16] In this paper, detailed data regarding this phase transition such as variations in crystal structures, electronic states, and magnetic properties are reported and the mechanism of this phase transition is discussed.

2. Experimental Section

Rubidium(I) manganese(II) hexacyanoferrate(III) was prepared by reacting an aqueous solution (0.1 mol dm^{-3}) of $MnCl_2$ with a mixed aqueous solution of RbCl (1 mol dm^{-3}) and $K_3[Fe(CN)_6]$ (0.1 mol dm^{-3}) to yield a precipitate. The precipitate was filtered and dried and yielded a powdered sample.

Elemental analyses of Rb, Mn, and Fe in the synthesized compound were performed by inductively coupled plasma mass spectrometry (ICP-MS). The morphology of the compound was measured by a Hitachi S 4200 scanning electron microscope (SEM) with 3.5 kV accelerating voltage, and 30 μA of beam current was used for imaging. The X-ray photoelectron spectroscopy (XPS) measurements were conducted using a Physical Electronics odel 5600 spectrometer equipped with a hemispherical capacitor analyzer. Ultraviolet−visible (UV−vis) reflectance spectra and infrared (IR) spectra were recorded on a Shimadzu UV-3100 spectrometer and a Shimadzu FT-IR 8200PC spectrometer, respectively. For optical measurements, CaF_2 plates held the powder sample. The powder X-ray diffraction (XRD) patterns were measured with a Rigaku RINT2100 instrument (Cu Kα), and the powder sample was placed on a Cu plate. The magnetic properties were measured using a Quantum Design MPMS-7S superconducting quantum interference device (SQUID) magnetometer. The heat capacity was measured using a Quantum Design 6000 physical property measurement system (PPMS), and the data was collected during heating since the equipment used the thermal relaxation method.

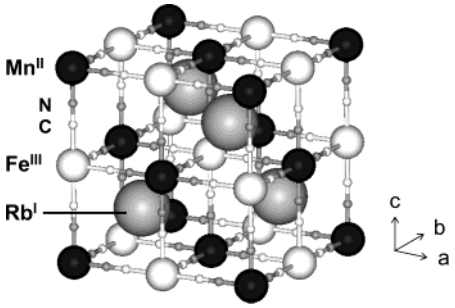

Figure 1. Schematic structure of $Rb^IMn^{II}[Fe^{III}(CN)_6]$. Large gray circles are Rb^I ions. Middle black circles are Mn^{II} ions, and middle white circles are Fe^{III} ions. Small white circles are C atoms, and small gray circles are N atoms.

3. Results

3.1. Material. The prepared compound was a light brown powder, and elemental analyses for Rb, Mn, and Fe indicated that the obtained precipitate had a formula of $RbMn[Fe(CN)_6]$ (Calcd: Rb, 24.26; Mn, 15.59; Fe, 15.85%. Found: Rb, 24.25; Mn, 15.95; Fe, 15.35%). The 1:1:1 ratio of Rb:Mn:Fe allowed the Mn ions to coordinate six cyanonitrogen, and consequently the network does not contain water molecules as shown in Figure 1. Other Prussian blue analogues have also been reported to have this type of crystal structure.[17] SEM images showed that the obtained powder sample was composed of cubic microcrystals that were 2.1 $\pm$ 1.1 μm (Figure 2).

3.2. SQUID Measurement. Figure 3 shows the product of the molar magnetic susceptibility (χ_M) and the temperature (T) vs T plots. The $\chi_M T$ value in the high-temperature (HT) phase was 4.67 cm^3 K mol^{-1} at 330 K, but when the sample was cooled at a cooling rate of 0.5 K min^{-1}, the $\chi_M T$ value decreased around 235 K and at T = 180 K in the low-temperature (LT) phase reached 3.19 cm^3 K mol^{-1}. Conversely, as the sample in the LT phase was warmed at a

(14) (a) Ludi, A.; Güdel, H. U. *Struct. Bonding (Berlin)* **1973**, *14*, 1. (b) Mallah, T.; Thiébaut, S.; Verdaguer, M.; Veillet, P. *Science* **1993**, *262*, 1554. (c) Verdaguer, M.; Mallah, T.; Gadet, V.; Castro, I.; Hélary, C.; Thiébaut, S.; Veillet, P. *Conf. Coord. Chem.* **1993**, *14*, 19. (d) Entley, W. R.; Girolami, G. S. *Science* **1995**, *268*, 397. (e) Ferlay, S.; Mallah, T.; Ouahès, R.; Veillet, P.; Verdaguer, M. *Nature* **1995**, *378*, 701. (f) Sato, O.; Iyoda, T.; Fujishima, A.; Hashimoto, K. *Science* **1996**, *271*, 49. (g) Buschmann, W. E.; Paulson, S. C.; Wynn, C. M.; Girtu, M. A.; Epstein, A. J.; White, H. S.; Miller, J. S. *Adv. Mater.* **1997**, *9*, 645. (h) Ohkoshi, S.; Hashimoto, K. *Chem. Phys. Lett.* **1999**, *314*, 210. (i) Ohkoshi, S.; Abe, Y.; Fujishima, A.; Hashimoto, K. *Phys. Rev. Lett.* **1999**, *82*, 1285. (j) Verdaguer, M.; Bleuzen, A.; Marvaud, V.; Vaissermann, J.; Seuleiman, M.; Desplanches, C.; Scuiller, A.; Train, C.; Garde, R.; Gelly, G.; Lomenech, C.; Rosenman, I.; Veillet, P.; Cartier, C.; Villain, F. *Coord. Chem. Rev.* **1999**, *190*, 1023. (k) Holmes, S. M.; Girolami, G. S. *J. Am. Chem. Soc.* **1999**, *121*, 5593. (l) Hatlevik, Ø.; Buschmann, W. E.; Zhang, J.; Manson, J. L.; Miller, J. S. *Adv. Mater.* **1999**, *11*, 914. (m) Ohkoshi, S.; Mizuno, M.; Hung, G. j.; Hashimoto, K. *J. Phys. Chem.* **2000**, *104*, 9365.

(15) (a) Garde, R.; Desplanches, C.; Bleuzen, A.; Veillet, P.; Verdaguer, M. *Mol. Cryst. Liq. Cryst. Sci. Technol., Sect. A* **1999**, *334*, 587. (b) Ohkoshi, S.; Machida, N.; Zhong, Z. J.; Hashimoto, K. *Synth. Met.* **2001**, *122*, 523. (c) Rombaut, G.; Verelst, M.; Golhen, S.; Ouahab, L.; Mathoniere, C.; Kahn, O. *Inorg. Chem.* **2001**, *40*, 1151. (d) Zhong, Z. J.; Seino, H.; Mizobe, Y.; Hidai, M.; Fujishima, A.; Ohkoshi, S.; Hashimoto, K. *J. Am. Chem. Soc.* **2000**, *122*, 2952. (e) Larionova, J.; Gross, M.; Pilkington, M.; Andres, H.; Stoeckli E. H.; Güdel, H. U.; Decurtins, S. *Angew. Chem., Int. Ed.* **2000**, *39*, 1605. (f) Podgajny, R.; Korzeniak, T.; Balanda, M.; Wasiutynski, T.; Errington, W.; Kemp, T. J.; Alcock, N. W.; Sieklucka, B. *Chem. Commun.* **2002**, *10*, 1138. (g) Li, D.; Gao, S.; Zheng, L.; Tang, W. *J. Chem. Soc., Dalton Trans.* **2002**, *14*. 2805. (h) Arimoto, Y.; Ohkoshi, S.; Zhong, Z. J.; Seino, H.; Mizobe, Y.; Hashimoto, K. *J. Am. Chem. Soc.* **2003**, *125*, 9240.

(16) Ohkoshi, S.; Tokoro, H.; Utsunomiya, M.; Mizuno, M.; Abe, M.; Hashimoto, K. *J. Phys. Chem. B* **2002**, *106*, 2423.

(17) Entley, W. R.; Girolami, G. S. *Inorg. Chem.* **1994**, *33*, 5165.

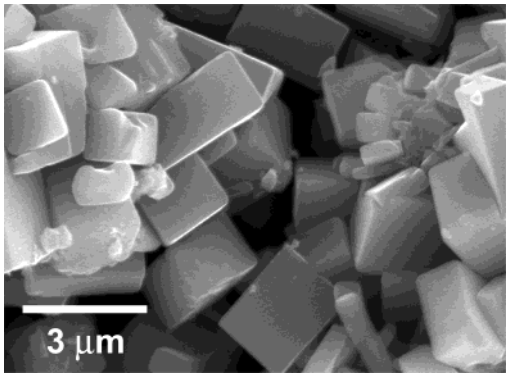

Figure 2. SEM image of the precipitate.

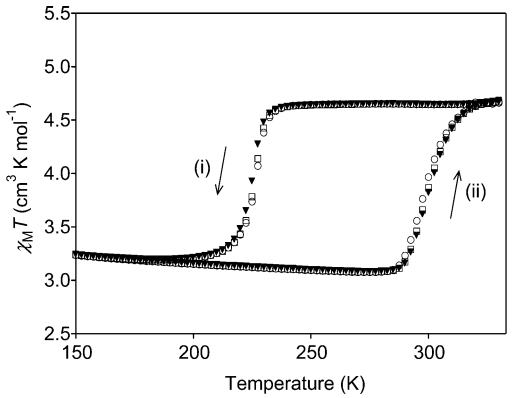

Figure 3. The observed $\chi_M T-T$ plots in the cooling (i) and warming (ii) processes, first measurement (○), second measurement (□), and third measurement (▼).

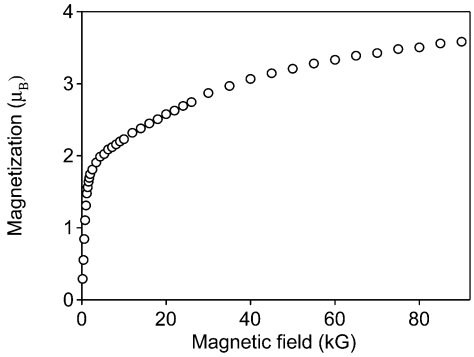

Figure 4. Magnetization vs external magnetic field plots of the LT phase at 3 K.

heating rate of 0.5 K min^{-1}, the $\chi_M T$ value suddenly increased near 285 K and reached the HT phase value at 325 K. The transition temperatures from HT to LT ($T_{1/2\downarrow}$) and from LT to HT ($T_{1/2\uparrow}$) were 225 and 300 K, respectively, and the width of the thermal hysteresis loop ($\Delta T = T_{1/2\uparrow} - T_{1/2\downarrow}$) was 75 K. This temperature-induced phase transition was repeatedly observed. Furthermore, when the LT phase was cooled to a very low temperature under an external magnetic field of 10 G, it exhibited spontaneous magnetization with a Curie temperature (T_C) of 12 K. The magnetization as a function of the external magnetic field at 3 K indicated that the saturated magnetization (M_s) value was 3.6 μ_B (Figure 4) and the coercive field (H_c) value was 1050 G (Figure 5). The $\chi_M^{-1}-T$ plots of the paramagnetic LT phase showed positive Weiss temperatures (Θ) between 12 and 15 K, which

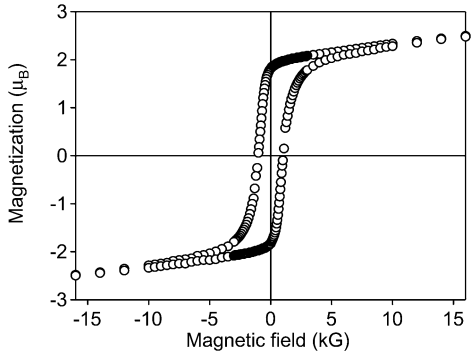

Figure 5. Magnetic hysteresis loop of the LT phase at 3 K.

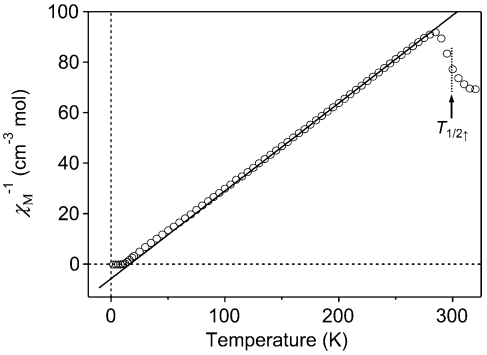

Figure 6. The observed $\chi_M^{-1}-T$ plots. The data between 150 and 270 K was fitted to Curie−Weiss plots (−).

Table 1. XPS Data of the HT and LT Phases

	binding energy [eV]			
	Fe ion		Mn ion	
compound	$2P_{1/2}$	$2P_{3/2}$	$2P_{1/2}$	$2P_{3/2}$
HT	724.1	710.1	654.0	641.8
LT	721.7	708.8	654.4	642.5
$K^I_3[Fe^{III}(CN)_6]$	723.6	710.0		
$K^I_4[Fe^{II}(CN)_6]$	721.8	709.1		

were obtained by extrapolating the data in the temperature region of 30−270 K and 150−270 K, respectively (Figure 6).

3.3. XPS, IR, and UV−Vis Reflectance Spectroscopy. The XPS spectra of $K^I_3[Fe^{III}(CN)_6]$, $K^I_4[Fe^{II}(CN)_6]$, HT, and LT phases were measured. In the HT phase, the Fe-$2P_{3/2}$ and Mn-$2P_{3/2}$ electron binding energies were 710.1 and 641.8 eV, respectively (Table 1). In the LT phase, the Fe-$2P_{3/2}$ and Mn-$2P_{3/2}$ electron binding energies were 708.8 and 642.5 eV, respectively. The $2P_{3/2}$ electron binding energies for the reference samples of $K^I_3[Fe^{III}(CN)_6]$ and $K^I_4[Fe^{II}(CN)_6]$ were 710.0 and 709.1 eV, respectively.

The IR spectra were recorded over a temperature range between 300 and 10 K. Figure 7 shows the CN^- stretching frequencies at 300, 240, 220, 200, and 10 K. At 300 K, a sharp CN^- peak was observed at 2152 cm^{-1} (line width = 9 cm^{-1}), and as the temperature decreased, the intensity of this peak decreased. Around 220 K a new broad peak appeared at 2095 cm^{-1} (line width = 65 cm^{-1}). These IR changes were in the same temperature range of the phase transition in the $\chi_M T-T$ plots.

Figure 8 shows the UV−vis reflectance spectra of the HT and LT phases. In the HT phase, the absorption bands were

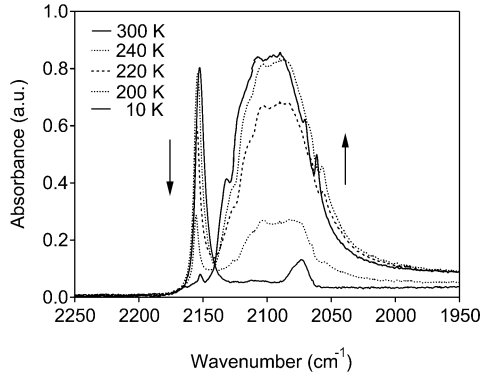

Figure 7. Temperature dependence of CN^- stretching frequencies in the IR spectra as the temperature decreases.

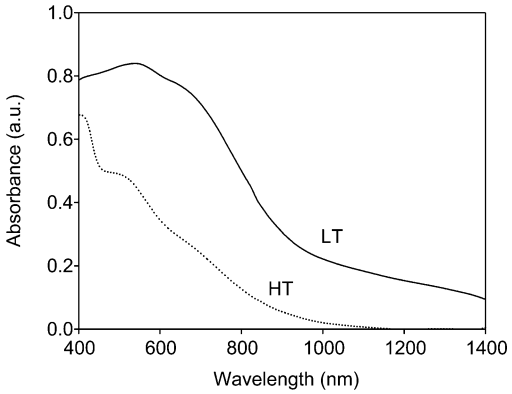

Figure 8. UV−vis reflectance spectra of the LT (solid line) and HT (dotted line) phases.

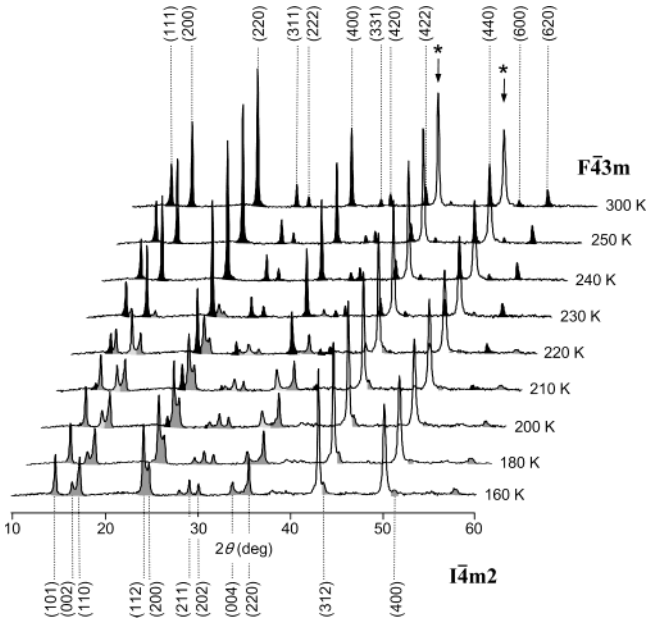

Figure 9. Temperature dependences of XRD spectra. Black and gray peaks are the diffraction peaks of the HT and LT phases, respectively, and light gray peak is the overlapped peak of the HT and LT phases. (* indicates Cu from the sample holder.)

approximately 410, 520, and 680 nm, while the band absorptions in the LT phase were 540, 700, and 1100 nm.

3.4. XRD Spectroscopy. Figure 9 shows the XRD patterns as the temperature decreased from 300, 250, 240, 230, 220, 210, 200, 180, to 160 K. The diffraction pattern of the HT phase was consistent with a face-centered cubic ($F\bar{4}3m$) structure with a lattice constant of 10.533 Å (at 300 K). As the sample was cooled, the XRD peaks of the HT phase decreased and different peaks appeared. The observed XRD pattern in the LT phase showed a tetragonal structure of $I\bar{4}m2$ with $a = b = 7.090$ Å and $c = 10.520$ Å (at 160 K), which correspond to $a = b = 10.026$ Å and $c = 10.520$ Å in a cubic lattice. The unit cell volume of 1169 $Å^3$ in the HT phase was reduced about 10% to 1057 $Å^3$ in the LT phase, and the tetragonal structure returned to the cubic one upon warming.

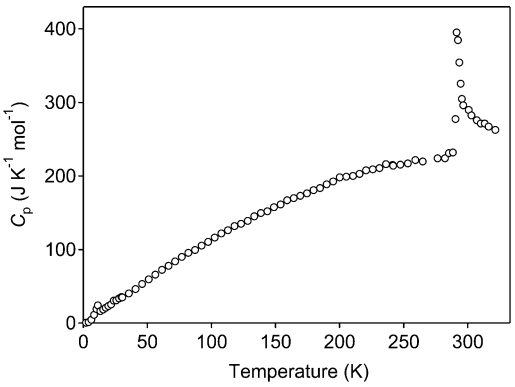

Figure 10. C_p vs T plots as the temperature increases.

3.5. Heat Capacity. The molar heat capacity (C_p) of this compound between 2 and 320 K was measured (Figure 10), and as the temperature increased, the heat capacity showed an anomalous peak in the temperature range of 290−300 K. A transition enthalpy (ΔH) of 1.7 kJ mol^{-1} and a transition entropy (ΔS) of 6 J K^{-1} mol^{-1} in this phase transition were obtained by eliminating the normal heat capacity of the LT phase.[18]

4. Discussion

4.1. Electronic States of HT and LT Phases. The observed Fe-$2P_{3/2}$ electron binding energy of 710.1 eV in the HT phase corresponds to an electron binding energy of 710.0 eV for Fe^{III} in $K^{I}_3[Fe^{III}(CN)_6]$. In contrast, the Fe-$2P_{3/2}$ binding energy of 708.8 eV in the LT phase is close to that of Fe^{II} in $K^{I}_4[Fe^{II}(CN)_6]$, 709.1 eV. The shift of the Mn-$2P_{3/2}$ binding energy from HT to LT phases suggests that the oxidation number of the Mn ion increases from II to III. The CN^- stretching peak at 2152 cm^{-1} in the HT phase is due to the CN^- ligand bridged to Fe^{III} and Mn^{II} ions ($Fe^{III}-CN^-Mn^{II}$), but the broad CN^- stretching peak at 2095 cm^{-1} in the LT phase is assigned to the CN^- ligand bridged to Fe^{II} and Mn^{III} ions ($Fe^{II}-CN^-Mn^{III}$). These XPS and IR spectra indicate that valence states for Mn and Fe ions in the HT phase are $Mn^{II}(d^5)$ and $Fe^{III}(d^5)$ and those in the LT phase are $Mn^{III}(d^4)$ and $Fe^{II}(d^6)$. Considering the decrease in the $\chi_M T$ value at $T_{1/2}$↓, the electronic states of the HT and LT phases are assigned to $Mn^{II}(d^5; S = {}^5/_2)-CN^-Fe^{III}(d^5; S = {}^1/_2)$ and $Mn^{III}(d^4; S = 2)-CN^-Fe^{II}(d^6; S = 0)$, respectively. These assignments are also supported by Mn and Fe X-ray emission

(18) To determine the excess heat capacity due to the observed thermal phase transition, the normal heat capacity curve was calculated by a least-squares fitting of $aT^2 + bT + c$, in the temperature region between 190 and 280 K.

Scheme 1. Reaction Scheme between the LT and HT Phases

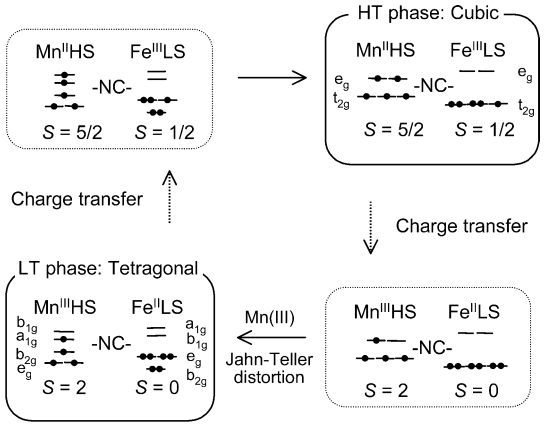

and absorption spectroscopies.[19] The structural change from cubic to tetragonal in the XRD measurement (Figure 9) is explained by the Mn^{III} Jahn−Teller transformation of the tetragonally octahedral elongation type (B_{1g} oscillator mode).[20−22] Thus, the d-orbitals for both metal ions in the LT phase have D_{4h} symmetry (a_{1g}, b_{1g}, b_{2g}, and e_g). Therefore, the precise electronic state of LT phase is $Mn^{III}(e_g^2b_{2g}^1a_{1g}^1$; $S = 2)$−NC−$Fe^{II}(b_{2g}^2e_g^4$; $S = 0)$ (Scheme 1).

The UV−vis reflectance spectra can be explained using the assigned electronic states for the HT and LT phases. Absorptions near 410 and 520 nm in the HT phase are due to a ligand-to-metal charge transfer of $[Fe^{III}(CN)_6]$ and d−d transition of Fe^{III} ($^2T_{2g} \rightarrow {}^4T_{1g}$), respectively.[23] In the LT phase, the absorptions around 540 nm ($^5B_{1g} \rightarrow {}^5B_{2g}$, ^5E_g) and 1100 nm ($^5B_{1g} \rightarrow {}^5A_{1g}$) are due to Jahn−Teller distorted Mn^{III},[20] and the broad absorption around 700 nm is from the metal-to-metal charge-transfer band (intervalence transfer band) in the mixed-valence compound.

4.2. Mechanism of Phase Transition. Prussian blue analogues are in class II mixed-valence compounds, which have the potential to exhibit a charge-transfer phase transition and are represented by two parabolic potential-energy curves due to valence isomers in the nuclear coordinate of the coupled vibrational mode.[3,4] When these two vibronic states interact, the ground state surface has two minima in the vibrational coordinate. In the present system, the Mn^{III}−Fe^{II} vibronic state is a ground state at $T = 0$ K for the vibrational coordinate (mixed-valency mode) (black curve in Figure 11a). Piepho, Krausz, and Schatz (PKS model) and Prassides studied this kind of diagram with two active modes.[3f,g] Moreover, in this situation, the Mn^{III} causes Jahn−Teller distortion, and the energy of the Mn^{III}−Fe^{II} has two minima as shown in the configurational coordinate (Jahn−Teller mode) (gray curve in Figure 11a). In the present system, Mn^{III} ions show an elongation-type Jahn−Teller distortion. These potential surfaces change as the temperature increases, which causes a phase transition. To understand the obtained results, the free energy changes of LT and HT phases were analyzed. The LT and HT phases consist of $D_{4h}Mn^{III}(^5B_{1g})$−$D_{4h}Fe^{II}(^1A_{1g})$ and $O_hMn^{II}(^6A_{1g})$−$O_hFe^{III}(^2T_{2g})$, respectively. The entropies due to the spin-multiplicities lead to a crossover from LT to HT phases as the temperature increases. Although the present compound does not show spin crossover, the entropy-induced phase transition is analogous to the phase transition of spin crossover complex. The free energies of the LT phase (G_{LT}) and HT phase (G_{HT}) depend on temperature as described in eq 1. The LT phase consists

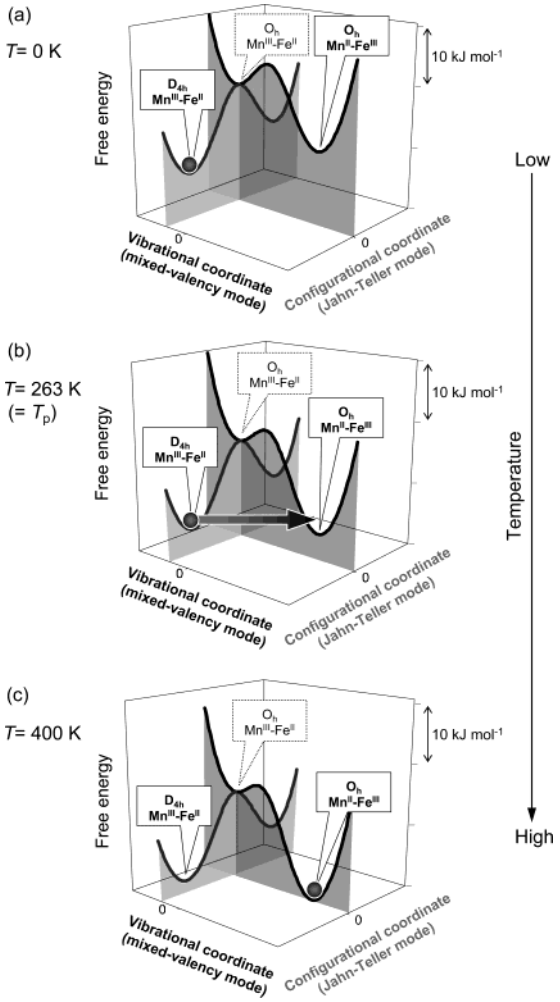

Figure 11. The schematic free energy surfaces of this system in mixed-valence (black curve) and Jahn−Teller (gray curve) modes: (a) ground state is Mn^{III}−Fe^{II} and metastable state is Mn^{II}−Fe^{III} at $T = 0$ K, (b) $T =$ 263 K ($=T_p$), (c) ground state is Mn^{II}−Fe^{III} and metastable state is Mn^{III}−Fe^{II} at $T = 400$ K. Each curve is calculated on the basis of eq 1. Gray spheres indicate population.

(19) (a) Osawa, H.; Iwazumi, T.; Tokoro, H.; Ohkoshi, S.; Hashimoto, K.; Shoji, H.; Hirai, E.; Nakamura, T.; Nanao, S.; Isozumi, Y. *Solid State Commun.* **2003**, *125*, 237. (b) Yokoyama, T.; Tokoro, H.; Ohkoshi, S.; Hashimoto, K.; Okamoto, K.; Ohta, T. *Phys. Rev. B* **2002**, *66*, 184111.

(20) (a) Davis, T. S.; Fackler, J. P.; Weeks, M. J. *Inorg. Chem.* **1968**, *7*, 1994. (b) Doddrell, D. M.; Bendall, M. R.; Pegg, D. T.; Healy, P. C.; Gregson, A. K. *J. Am. Chem. Soc.* **1977**, *99*, 1281. (c) Gerloch, M. *Inorg. Chem.* **1981**, *20*, 638. (d) Åkesson, R.; Pettersson, L. G. M.; Sandström, M.; Wahlgren, U. *J. Phys. Chem.* **1992**, *96*, 150. (e) Kück, S.; Hartung, S.; Hurling, S.; Petermann, K.; Huber, G. *Phys. Rev. B* **1998**, *57*, 2203. (f) Krzystek, J.; Telser, J.; Pardi, L. A.; Goldberg, D. P.; Hoffman, B. M.; Brunel, L. C. *Inorg. Chem.* **1999**, *38*, 6129.

(21) Moritomo, Y.; Kato, K.; Kuriki, A.; Takata, M.; Sakata, M.; Tokoro, H.; Ohkoshi, S.; Hashimoto, K. *J. Phys. Soc. Jpn.* **2002**, *71*, 2078.

(22) The precise bond lengths of the LT phase were determined by synchrotron radiation X-ray powder structural analysis. The two long and four short Mn−N bond distances are 2.26(2) and 1.89(3) Å, respectively, and the two short and four long Fe−C bond distances are 1.89(2) and 2.00(3) Å, respectively.[21]

(23) Naiman, C. S. *J. Chem. Phys.* **1961**, *35*, 323.

$$G_i = H_i - S_i T \qquad (i = \mathrm{LT, HT}) \qquad (1)$$

of $Mn^{III}(^5B_{1g})$ and $Fe^{II}(^1A_{1g})$, and $^5B_{1g}$ has 5(= 1 (orbital degeneracy) × 5 (spin multiplicity))-fold degeneracy and $^1A_{1g}$ has 1(= 1 × 1)-fold degeneracy, respectively. Consequently, the degeneracy of the LT phase is 5(= 5 × 1)-fold. In contrast, since the HT phase consists of $Mn^{II}(^6A_{1g})$ and $Fe^{III}(^2T_{2g})$, and $^6A_{1g}$ has 6(= 1 × 6)-fold degeneracy and $^2T_{2g}$ has 6(= 3 × 2)-fold degeneracy, the degeneracy of the HT phase is 36(= 6 × 6)-fold. Therefore, their entropies (S_{LT} and S_{HT}) are $S_{LT} = R \ln 5$ and $S_{HT} = R \ln 36$, respectively. When the cooperative force between converted sites, e.g., elastic interaction, is neglected, the ΔS in this phase transition is $R \ln (36/5) = 16.4$ J K^{-1} mol^{-1}. From eq 1, the transition temperature (T_p) of the phase transition can be obtained by $\Delta H/\Delta S$. Here, T_p of this system is defined as $T_p = (T_{1/2\downarrow} + T_{1/2\uparrow})/2 = 263$ K. Using $T_p = 263$ K and $\Delta S = 16.4$ J K^{-1} mol^{-1}, ΔH was 4.3 kJ mol^{-1}. G_{LT} and G_{HT} change as the temperature increases and a phase transition occurs at T_p. In addition, Figure 11b and Figure 11c show the G_{LT} and G_{HT} surfaces in the vibrational (mixed-valency mode) and configurational (Jahn−Teller mode) coordinates at each temperature. The heat capacity measurement showed $\Delta H = 1.7$ kJ mol^{-1} and $\Delta S = 6$ J K^{-1} mol^{-1}, which are smaller than theoretical values since the orbital contribution to the entropy of Fe^{III} in the HT phase becomes smaller. The extended X-ray absorption fine structure data of the HT phase shows a small distortion in the octahedral coordinates of metal ions, which is probably due to the small contribution of LT phase.[19b] In this situation, $^2T_{2g}$ of Fe^{III} is reduced to $^2B_{2g}$. Then ΔS and ΔH are changed to $R \ln (12/5) = 7.28$ J K^{-1} mol^{-1} and 1.9 kJ mol^{-1}, respectively, which are close to the experimental values.

5. Conclusion

In summary, a temperature-induced phase transition in $RbMn[Fe(CN)_6]$ ($T_{1/2\downarrow} = 225$ K, $T_{1/2\uparrow} = 300$ K) was observed with a large thermal hysteresis loop of 75 K. The charge transfer from Mn^{II} to Fe^{III} accompanying the Jahn−Teller effect on the $Mn^{III}N_6$ moiety explains this phase transition. Recently, the photoinduced phase transition from the LT to HT phases has been also observed in this system.[24] These thermally induced and optical phase transition phenomena are due to the bistability in the electronic state and the strong cooperativity in CN^- bridged 3-D structure.[14,15] Since new building blocks for cyanide-bridged metal complexes are currently being prepared,[25] various phase transition phenomena will be observed with cyanide-bridged metal complexes in the near future.

Acknowledgment. The present research is supported in part by a Grant for 21st Century COE Program "Human-Friendly Materials based on Chemistry" and a Grand-in-Aid for Scientific Research from the Ministry of Education, Culture, Sports, Science, and Technology of Japan.

IC030332F

(24) Tokoro, H.; Ohkoshi, S.; Hashimoto, K. *Appl. Phys. Lett.* **2003**, *82*, 1245.

(25) (a) Beauvais, L. G.; Long, J. R. *J. Am. Chem. Soc.* **2002**, *124*, 2110. (b) Lescouëzec, R.; Vaissermann, J.; Lloret, F.; Julve, M.; Verdaguer, M. *Inorg. Chem.* **2002**, *41*, 5943. (c) Bennett, M. V.; Long, J. R. *J. Am. Chem. Soc.* **2003**, *125*, 2394. (d) Smith, J. A.; Galán-Mascarós, J. R.; Clérac, R.; Sun, J. S.; Ouyang, X.; Dunbar, K. R. *Polyhedron* **2001**, *20*, 1727.